



Enhancement of piezoelectric energy-harvesting capacity of electrospun β -PVDF nanogenerators by adding GO and rGO

Merve Zeyrek Ongun¹ · Sibel Oguzlar² · Eyyup Can Doluel³ · Ugur Kartal³ · Metin Yurddaskal⁴

Received: 7 August 2019 / Revised: 26 November 2019 / Accepted: 6 December 2019 / Published online: 18 December 2019
© Springer Science+Business Media, LLC, part of Springer Nature 2019

Abstract

In this paper, the electrical output voltage of highly piezoelectric properties of polyvinylidene fluoride (PVDF) was enhanced by using graphene oxide (GO) and reduced graphene oxide (RGO) additives. GO and RGO materials were synthesized by Hummer's method and their morphology, crystallinity and the effect of electrical outputs of β -PVDF were investigated. Different amounts of GO and RGO additives (0.4 and 0.8 wt%) embedded in PVDF polymeric material and electrospun nanofibres that show piezoelectric features were prepared by electrospinning process. All of the produced nanofibres were characterized in terms of structural and morphological properties by using Fourier transform infrared spectroscopy (FTIR), X-ray diffraction (XRD) and scanning electron microscopy (SEM). The piezoelectric nanogenerators prepared using electrospun β -PVDF mats with different amounts of GO and RGO were fabricated by sandwiching between two conductive aluminium plates. The same dimension (4 cm \times 5 cm) of nanogenerators with a mat thickness of 50 μ m was used to evaluate the electrical output data. All of the produced nanogenerators were examined for a finger-tapping action with a frequency of \sim 5 Hz. It was observed that the presence of 0.8 wt% of RGO increased the open-circuit voltage of β -PVDF for approximately nine times. This enhancement is associated with a certain and powerful interfacial interaction that occurs within the adsorption of molecular chain conformation of β -PVDF onto the GO and RGO surfaces. This new type of RGO-based nanogenerator could be of great advantage for a wide range of applications such as a self-charging power source, flexible and stretchable electronic devices, energy-harvesting devices, sensors and other electronic-based systems

1 Introduction

Piezoelectric materials have great importance due to their high-energy conversion capability from mechanical energy to electrical energy and vice versa. When they are subjected to the mechanical stress, they produce electrical voltage mentioned as the direct piezoelectric effect, and also, in the converse-piezoelectric effect they generate mechanical charge from an electrical field [1]. Piezoelectric materials are used in many applications such as damage detections

[2], automotive engines [3], pressure sensors [4], actuators [5] and energy harvesters [6]. Lead zirconate titanate (PZT) [7], barium titanate (BaTiO₃) [8], zinc oxide (ZnO) [9–14], aluminium nitride (AlN) [15–18] and polyvinylidene fluoride (PVDF) [19–26] are characteristic piezoelectric ingredients used in microelectromechanical system (MEMS) transducers.

Last decades, PVDF, referred as electroactive polymers (EAPs), has found wide application area as a piezoelectric composite because of its some excellent properties such as flexibility, high mechanical robustness, low stiffness and ease of processing at low temperatures. The PVDF exhibits five different polymorphs (α , β , γ , δ and ϵ) that related to the molecular chain conformation. Among these phases of PVDF, the β phase is the most important due to its spontaneous polarization, piezoelectric sensitivity and highest dipole moment per unit cell. Its output voltage depends on the electroactive phase and crystallinity. β -phase providing the highest polarization by stabilizing the all-trans chain conformation of the PVDF in the crystal unit, make it suitable in nanogenerator applications [27].

✉ Merve Zeyrek Ongun
merve.zeyrek@deu.edu.tr

¹ Technical Programs Department, Izmir Vocational High School, Dokuz Eylul University, Buca, Izmir, Turkey

² Center for Fabrication and Application of Electronic Materials, Dokuz Eylul University, Buca, Izmir, Turkey

³ The Graduate School of Natural and Applied Sciences, Dokuz Eylul University, Buca, Izmir, Turkey

⁴ Department of Metallurgical and Materials Engineering, Dokuz Eylul University, Buca, Izmir, Turkey

Many techniques have been used for inducing the formation of more polar β -crystal phases such as electrospinning [28], using nanoparticles, metal salts or ionic liquid additives [29–32], crystallization under high pressure [33], annealing [34], polymer poling [35], etc. Electrospinning has become a promising technique that provides the alignment of molecular dipoles with a single processing stage and the formation of β -phase that has all of the dipolar moments pointing to the same direction. Also, the piezoelectric potential of β -phase can be further enhanced with the incorporation of ferroelectric inorganic particles that have high dielectric constant such as zinc stannate (ZnSnO_3) [36], barium titanate (BaTiO_3) [37], lead zirconate titanate (PZT) [38], and lead magnesium niobate–lead titanate (PMN–PT) [39]. Despite the doping of the stannate and titanate derivative ceramic powders in the PVDF matrix, the dielectric constant of PVDF is not high enough due to the weak interfacial interaction between the porous structures of the ceramic powders and polymeric matrix [40–44]. In recent years, in the scientific world, the interest in carbon nanotubes has greatly increased due to yielded better mechanical features and dielectric properties because of their higher surface area [45, 46]. Single-layer graphite, known as graphene, has attracted considerable scientific interest in recent years owing to its outstanding mechanical, thermal and electrical properties as well as large surface area [47–49]. Thus, graphene has been considered to be an ideal nanofiller for improving the mechanical, electrical, and thermal properties of polymers [50]. Since graphene-based structures have hydrophobic layers which make the production of aqueous solutions of PVDF-graphene composites more difficult, graphene should be treated by an oxidation process to obtain graphene oxide (GO) which has more hydrophilic layered structure including functional groups like $-\text{OH}$ and $-\text{COOH}$. A reduction process should be applied to get reduced graphene oxide (RGO) by removing of some functional groups from the structure. It is noteworthy that the RGO is a carbonaceous material that shows very similar properties of graphene. Most of the research in this field has focused on GO or RGO thanks to their homogenous dispersion in the polymer [51–54].

Recently, the potential of graphene oxide and derivatives that provide an enhancement of the electrical output of PVDF-based nanogenerators has been investigated. This improvement is based on the development of β polymorph layout that shows piezoelectric performance on the main chain of PVDF, as a result of inducing the graphene and derivatives [55–61]. The electrical output values of generators produced by PVDF polymer in the presence of additives, except graphene and derivatives, were presented as the levels of mV by several types of research. However, Alamusu et al. [60] reported that they produced an open-circuit voltage of 4 V for PVDF samples with 0.2 wt% graphene

addition. Abolhasani et al. [62] explained that they obtained the open-circuit voltage of 3.8 and 7.9 V for un-filled and 0.1 wt% graphene-filled- β -PVDF nanofiber, respectively.

In light of the literature, the improvements of the electrical output of PVDF-based nanogenerators along with graphene derivatives encouraged us to think about possible and powerful interfacial interactions within the adsorption of the molecular chain conformation of β -PVDF onto the GO and RGO surfaces. Therefore, we aimed to produce GO- and RGO-filled β -PVDF nanofibres with higher electrical output compared to the free β -PVDF nanogenerators. Besides, we investigated the influence of the amounts of GO and RGO, which have been prepared by modified Hummer's method, on the piezoelectric ability of β PVDF nanofibres. Herein, we report the development of nanofiber-based PVDF/RGO and PVDF/GO nanogenerators with extremely high electrical output values.

2 Materials and methods

2.1 Reagents

All of the solvents and chemicals used were analytical grade. Poly(vinylidene fluoride) (PVDF) with a molecular weight of repeat unit 64.03 (g/mol) was purchased from Sigma-Aldrich. The solvent *N,N*-Dimethylformamide (DMF), purity 99.5%, and acetone were supplied by Fluka. Hydrazine hydrate (N_2H_4 , 100%) was supplied by Sigma-Aldrich. Graphite flakes were provided from Selen Chemistry. Potassium permanganate (KMnO_4 , 99%) was purchased from Edukim. Hydrogen peroxide (H_2O_2 , 35%) and sulphuric acid (H_2SO_4 , 95–97%) were purchased from Merck. Hydrochloric acid (HCl, 30–32%) was supplied by Sigma-Aldrich.

2.2 Instrumentation

For the preparation of the electrospun nanofibres, a programmable syringe pump (Top-5300) and a high-voltage power supply (Gamma High Voltage ES30) were used. Phase identification and crystal structures of synthesized GO and RGO samples were carried out through a Thermo Scientific ARL X-ray diffractometer (XRD) which works with voltage and current settings of 40 kV and 30 mA, respectively, and uses $\text{Cu-K}\alpha$ radiation (1.5405 Å). Microstructure images were captured at different magnifications by using a JEOL JSM 6060 scanning electron microscope (SEM) with 20 kV accelerating voltage. The dielectric constant and dielectric loss of NGs were measured by an impedance analyzer (Alpha-A High Performance Frequency Analyzer, Novocontrol) between 10^2 and 10^6 Hz. In this study, output voltage data of the electrospun β -PVDF nanofibres were

measured as peak-to-peak amplitude values by using the digital oscilloscope (AATech ADS-1022B - Digital Storage Oscilloscope).

2.3 Synthesis of GO and RGO

Graphene oxide was synthesized by modified Hummer's method. In this method, H_2SO_4 and graphite flakes in the ice bath were stirred on a magnetic stirrer for 30 min at 600 rpm. KMnO_4 was added slowly into this mixture and the temperature was kept at under 20 °C degree; this mixture was stirred for 3 h. Distilled water was added dropwise to dilute the solution and the temperature was maintained below 50 °C. Then 100 ml of distilled water was added suddenly to finish the oxidation. The solution is continuously stirred until its colour of brown. H_2O_2 was added slowly and this solution stirred for 1 h. The solution centrifuged with HCl and distilled water (1:9) solution to separate synthesized GO and excess materials/precursors/chemicals six times at 5000 rpm for 10 min. After this centrifuged process, the obtained moist GO powder was dried in the oven at 100 °C. GO was reduced by a chemical method to obtain RGO with reflux technique. In this reduction process, N_2H_4 was used as the reducing agent. GO and distilled water were taken in a round-bottom flask. The solution was stirred to obtain a homogeneous solution and N_2H_4 was added into the solution dropwise. After the pre-stirring process, the solution was continuously stirred for 12 h at 80 °C. RGO powders were obtained successfully following these processes.

2.4 Solution preparation

In this study, 10% (w/v) of PVDF solution was used for electrospinning. Measured amounts of PVDF were ultrasonically stirred in a 10 ml of DMF/acetone mixture (1:1 by v/v) for 2 h at 80 °C until a transparent and homogeneous polymer solution was formed. The solution was cooled to ambient temperature. And then, the synthesized GO and RGO nanoparticles were added into the polymeric matrix in order to enhance the piezoelectric features of the PVDF. The optimal quantities of the additives in the cocktail composition were investigated by different amounts of the synthesized GO and RGO-NPs. For the preparation of two different concentrations (0.4 and 0.8 wt%) of GO- and RGO-NPs-filled PVDF composites, 4 and 8 mg of additives were added by to the PVDF (10% by w/v) solution. The cocktails were stirred under magnetic stirring for 2 h and kept ready for the electrospinning process.

2.5 Electrospinning process

Electrospinning technique was used to fabricate PVDF-based piezoelectric nanofiber. The polymer solutions were

placed in a 10-ml plastic syringe fitted with a metallic needle of 0.4 mm of inner diameter. The syringe was fixed vertically on the syringe pump and the electrode of the high-voltage power supply was clamped to the tip of the metal needle. The feed rate of the polymer solution was 2.0 ml/h, the applied voltage was between 20 and 25 kV and the tip-to-plate distance was set at 10 cm. All of the prepared solutions were loaded into the syringe having an attached needle. When the high voltage is applied between the needle and the aluminium substrate, the drop of the polymers becomes charged, reorients depending on the electric field and is collected on an electrically grounded metal plate in the form of nanofibres. The β -phase PVDF nanofibres were prepared by using the electrospinning process. Therefore, the electrospinning of PVDF provides the orientation of atoms from the nonpolar α -phase to the polar β -phase.

2.6 Fabrication of GO- and RGO-based PVDF nanogenerator

The simply piezoelectric nanogenerator devices were prepared by sandwiching the un-filled and varying amounts of graphene oxide and reduced graphene oxide-filled β -PVDF nanofibres as a dielectric material between two conductive aluminium plates. To evaluate the electrical output data of fabricated nanogenerators, the same dimension ($4 \times 5 = 20 \text{ cm}^2$) of active layers with a thickness of 50 μm was used. The nanogenerator (NG) produced from free-PVDF nanofiber; named PVDF-NG. The nanogenerators fabricated with PVDF electrospun fibers, which includes 0.4 and 0.8 wt% of the GO and RGO named 0.4-GONG, 0.8-GONG, 0.4-RGONG, and 0.8-RGONG, respectively. To investigate the effect of various amounts of GO and RGO on the open-circuit voltage (V_{oc}) of PVDF-based electrospun mats, a digital oscilloscope was used. Also, the dielectric constant and the dielectric loss of the NGs were measured by using impedance analyzer (See in Fig. 1).

3 Results and discussion

3.1 Characterization studies

3.1.1 XRD analysis

X-ray diffraction (XRD) patterns of graphite, RGO and GO are shown in Fig. 2a. The characteristic peak of graphite is clearly seen at 2θ of 26.44° which corresponds to an inter-layer spacing of 3.37 Å for the (002) reflection. Following the oxidation of graphite layers, the diffraction peak is obtained at 12.14°. During the process of reduction of GO, oxygen-containing functional groups are removed from the structure and disruption of the regular stacking of the GO

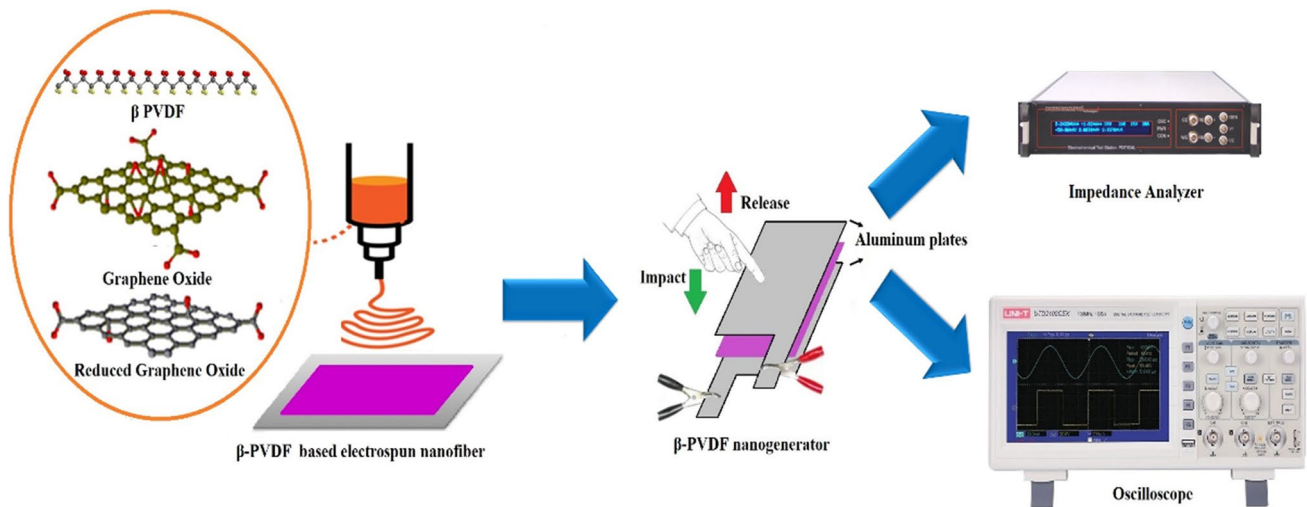


Fig. 1 Schematic scheme of fabrication and application of the experimental procedure for β -PVDF-based nanogenerators

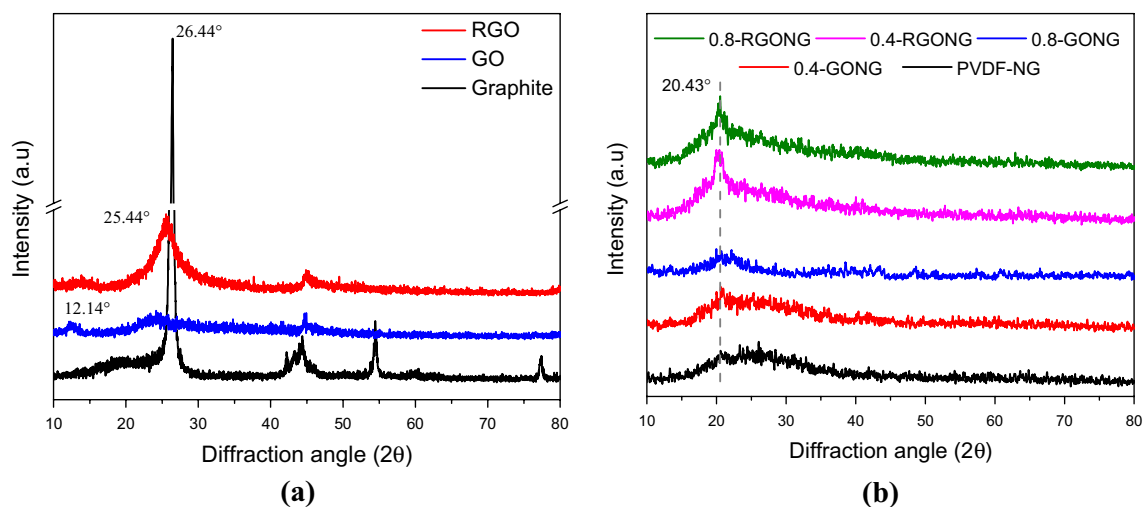


Fig. 2 XRD patterns of **a** produced additives, **b** β -PVDF electrospun mats depending on filler type and ratio

layers, which causes the disappearing of the peak at 12.14° . The disappearing of this peak also led to formation of a new splay peak between 17° and 31° which has maximum intensity at 2θ of 25.54° [63].

XRD analysis for the electrospun NG was carried out in the range of 10° to 80° as illustrated in Fig. 2b. The diffraction peak at 2θ of 20.43° attributed to the characteristic β -phase of PVDF and associated with (110) and (200) crystalline planes [64]. RGO has a much greater effect on increasing the β -peak intensity. This situation could be explained with the interaction between PVDF and RGO. During the electrospinning process, molecular chains of PVDF are stretched by the applied electric field. Thus, $-\text{CH}_2$ dipole of RGO and $-\text{CF}_2$ dipole of PVDF orientate together to build up a composed structure. The reason for the lack of

sharp peaks in the XRD patterns is due to the use of a small amount of RGO addition in accordance with the literature [61, 62].

3.1.2 FTIR analysis

Different crystalline phases of β -PVDF absorb different infrared wavelengths. It is known that the piezoelectric properties come from the β -phase of the PVDF [65]. Figure 3 shows the FTIR spectra of free β -PVDF and both GO- and RGO-filled PVDF electrospun nanofibres. As demonstrated in Fig. 3, the characteristic absorption bands of the β -phase of PVDF nanofibres refer to the piezoelectric crystalline phases that appeared at 840 and 1279 cm^{-1} . The addition of GO and RGO further enhanced the β phase of the PVDF

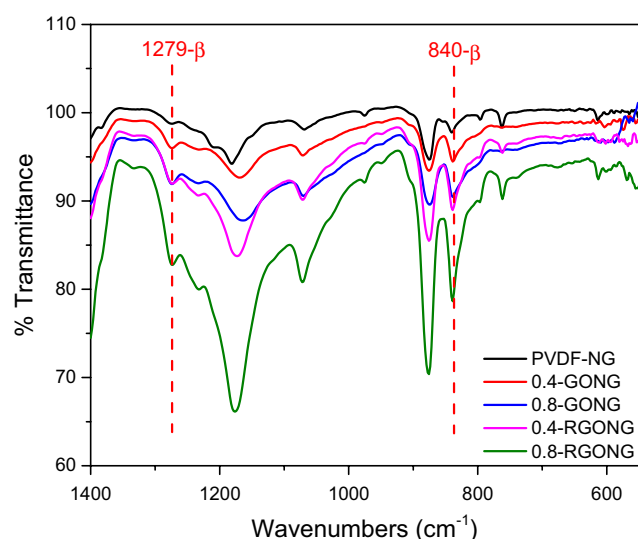


Fig. 3 FTIR spectra for PVDF-NG, GONG and RGONG electrospun mats

polymer. Five measurements were performed as PVDF-NG, 0.4-GONG, 0.4-RGONG, 0.8-GONG and 0.8-RGONG, respectively, in order to calculate the effective $\%(w/v)$ ratio. In the case of RGO filled, the intensity of β -PVDF characteristic bands was significantly improved especially for 0.8% (w/v) . It is also obvious from FTIR measurements that the β -phase stabilization and nucleation is more accelerated by GO and RGO.

3.1.3 Morphological analysis

Figure 4 shows the microstructure of PVDF-NG, GONG, and RGONG, respectively. It can be seen from the SEM images that GO and RGO homogeneously dispersed in PVDF thanks to their similar structures such as carbon-based structure and functional groups (carboxyl, hydroxyl). The obtained smooth and homogenous morphologies could be attributed to the π -stacking structure of GO and RGO. In addition, there are no cracks observed on the surface thanks to the flexible structure of NG mats. It can be easily seen from Fig. 4 that the pure PVDF-NG and RGONG have homogeneously formed bead-free nanofibres. However, there are some beads formed on the nanofibres in the structure of NG mats with the increasing addition of the GO. This phenomenon could be explained by the packaging of the GO nanosheets inside the nanofibres [66]. The electrospun GONG and RGONG mats were built of randomly oriented nanofibres with between diameters of 40–70 nm and 35–150 nm, respectively. Distribution of diameters of nanofibres was investigated by using a software as shown in SEM images in Fig. 4. It was obtained that the diameters of the nanofibres

were decreased with the increasing amount of fillers, which attributes to the decrease of viscosity [67].

3.2 Enhanced dielectric properties of electrospun mats

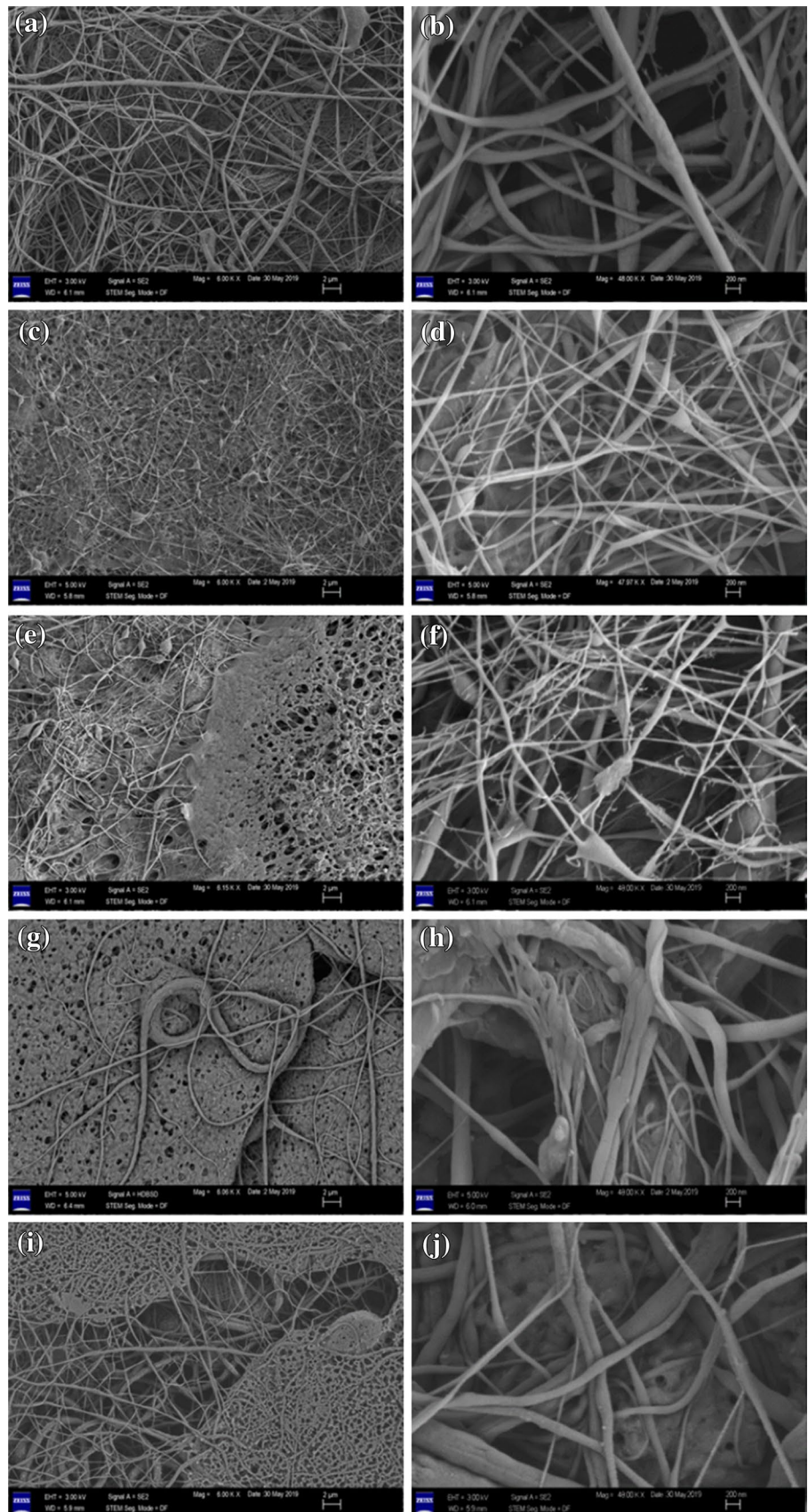
The dielectric properties of the electrospun mats with various GO and RGO concentrations were measured at room temperature as a function of frequency in the range of 10^2 – 10^6 Hz and are shown in Fig. 5. It can be seen from Fig. 5a that the dielectric constant values of PVDF-NG, 0.4GONG, 0.4RGONG, 0.8-GONG and 0.8-RGONG are 9.45, 24.45, 21.31, 27.60 and 35.16 at 10^3 Hz, respectively. These results show that the dielectric constant of 0.8-RGONG is approximately four times higher than that of PVDF-NG at 10^3 Hz. Thus, the RGO contribution is more effective in improving the dielectric constant than the GO contribution. In addition, the dielectric constants of the NGs are independent of the frequency. Basically, the nanofiller contribution rates, type of nanofillers and dispersion of nanofillers have significant effects on the dielectric constant of NGs. This increase can be attributed to the formation of micro capacitors in NGs. The increasing amount of GO/RGO causes the formation of micro capacitors which increases the dielectric constant in accordance with the literature just as some researchers observed in their studies [68–71]. However, there are few studies about the decreasing dielectric constants with different additives due to agglomeration and nonhomogenous dispersion of fillers [72].

Figure 5b shows the dielectric losses of NGs, which are around 0.01 at 10^4 Hz. The dielectric loss mechanisms of GONG and RGONG can be explained by interfacial polarization and electronic dipole polarization between β -PVDF and GO/RGO. Interface polarization occurs when neighbouring phases have different dielectric constant values. The functional groups present on the surface of GO do not prevent the formation of interfaces between GO and β -PVDF. The electrophilic fluorines in the molecular structure of β -PVDF can cause electronic dipole polarization. Besides, unsaturated coordination and dangling band atoms on the surface of the β -PVDF/RGO composites may result in orientational polarization which is the cause for dielectric loss [73, 74].

3.3 Output voltage measurements of graphene-based nanogenerators

The open-circuit voltages of nanogenerators have a complicated relationship with various determinants such as the diameter of nanofibres and conductivity of electrospun mat, the filler amounts of GO/RGO and impact frequency. The output voltage changes of all the NGs were measured by finger-tapping action with a frequency of ~ 5 Hz, as

Fig. 4 SEM images under 6k and 48k magnifications of **a, b** PVDF-NG, **c, d** 0.4-GONG, **e, f** 0.8-GONG, **g, h** 0.4-RGONG, **i, j** 0.8-RGONG



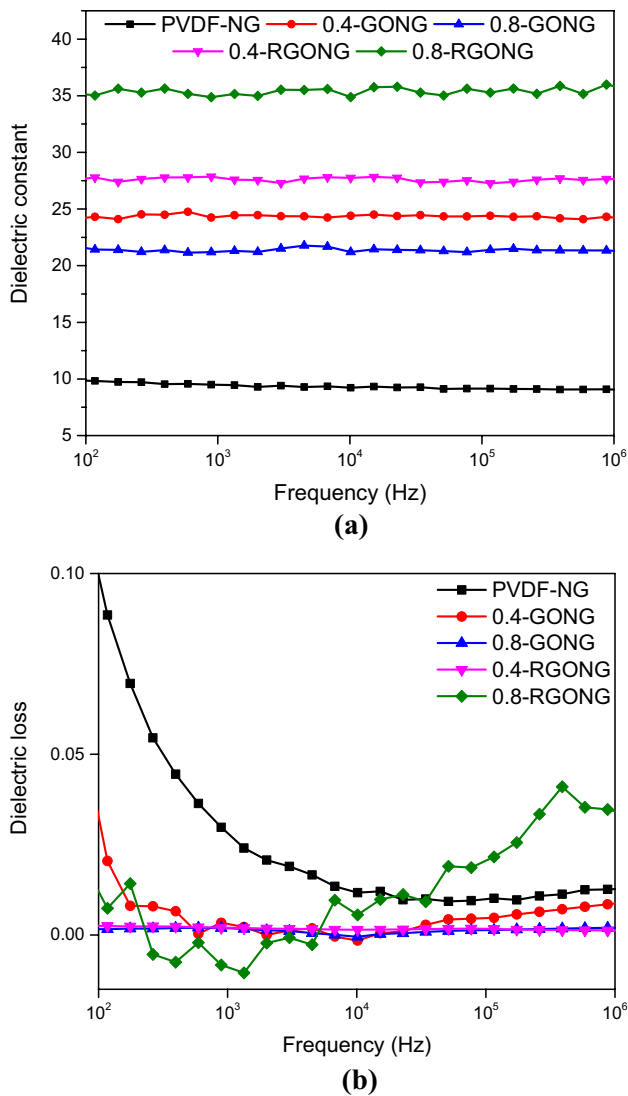


Fig. 5 Comparison of **a** dielectric constant and **b** dielectric loss of NGs

the impact-release process. When the nanogenerators were exposed repeatedly press-release cycles by the human finger, free electrons gathered at the interface of electrodes, and the open-circuit voltage occurred due to the accumulated electron transition across the electrodes and created a positive voltage peak. [62]. Figure 6 indicates the graphs of the output voltage changes of the PVDF, GO- and RGO-filled PVDF nanogenerators obtained with finger-tapping action. The V_{oc} of 0.8-RGONG, 0.4RGONG, 0.8-GONG, 0.4-GONG and PVDF-NG was calculated as an average voltage for five measurements and found as 4.38, 3.40, 0.65, 1.15 and 0.50 V, respectively. RGONG displayed certainly higher voltage than the other nanogenerators. It can be seen that the presence of 0.8 wt% RGO in β -PVDF nanofibres increased open-circuit voltage from 0.50 to 4.38

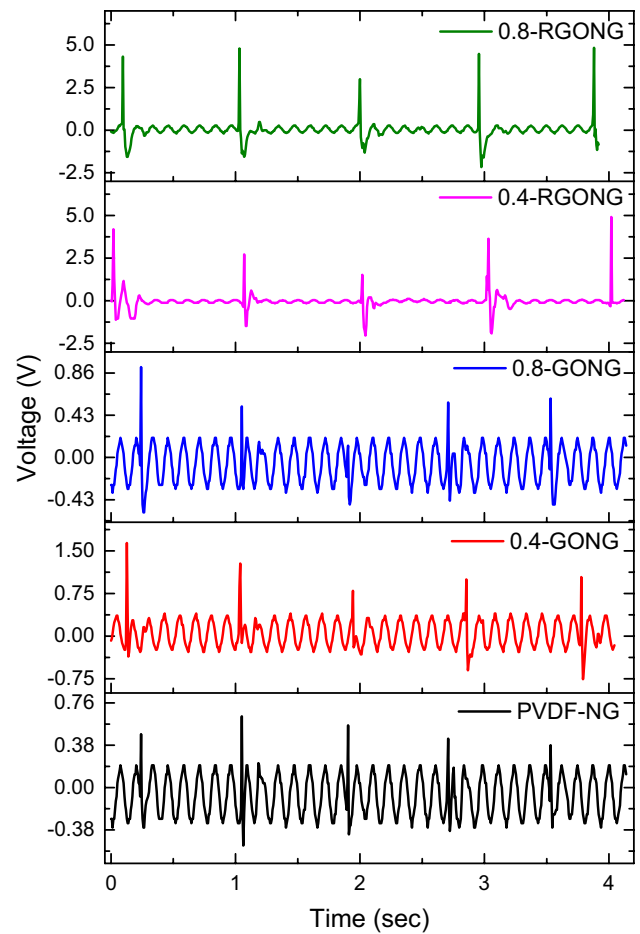


Fig. 6 Output voltage values induced upon press-hold-release process with a frequency of ~ 5 Hz

V, when compared with free β -PVDF. The increases in the output voltage of RGONGs are thought to originate from fewer functional groups attached to carbon atoms in the structure of reduced graphene oxide when compared with the graphene oxide structure. In this way, electron movement across the carbon atoms can occur at high speed. In addition, the high velocity flow of electrons has not been seen in the graphene oxide-filled PVDF nanogenerators. Despite the increase in the percentage of graphene oxide in the nanogenerator structure, 0.8-GONG gave the lowest electrical output voltage. Since 0.8-GONG has more functional groups attached to carbon atoms than 0.4-GONG, it is thought that the electron flow in this structure is prevented. The graphene oxide and derivatives enhance the electrical behaviour of the PVDF matrix because of having an unusually large surface area [75]. Besides, the compatibility between GO/RGO and β -PVDF is very high due to the presence of oxygen-containing functional groups on the surfaces of the GO and RGO. It is thought that the homogenous distribution of GO and RGO structures

within the β -PVDF improves the electron transfer on the polymeric chain.

4 Conclusion

In summary, the graphene derivatives are fully dispersed and well interacted with the polymer matrix because the synthesized GO and RGO nanoparticles have compatibility specification with PVDF. By using 0.4 and 0.8 wt% of these nanoparticles embedded in PVDF polymer, the highly flexible and stretchable nanosheets of GO/PVDF and RGO/PVDF were obtained by electrospinning technique. The electrospun β -PVDF mats were used to fabricate related nanogenerators by sandwiching between two conductive aluminium plates with the same dimension. The electrical outputs of the nanogenerators were evaluated using an oscilloscope for a finger-tapping action with a frequency of ~ 5 Hz. When compared with the free β -PVDF, in the presence of the 0.8 wt% of RGO, the highest enhancement electrical output voltage was obtained with an average positive voltage peak as 4.38 V. It is thought that the increment of the output voltage is mainly involved in interfacial interaction between β -PVDF and RGO nanoparticles. By the way, dielectric properties were enhanced significantly by the addition of GO and RGO in comparison to β -PVDF. Especially, the dielectric constant of 0.8-RGONG composite was increased to 35.16 which is approximately four times higher than that of PVDF-NG at 10^3 Hz. Also, dielectric losses of NGs were found around 0.01 at 10^4 Hz. The enhanced piezoelectric performances of the 0.8-RGONG allow the use of these nanogenerators as energy-harvesting devices, pressure sensors, portable electronics, and wearable devices.

Acknowledgements Synthesis and characterization measurements were performed at Dokuz Eylul University in Center for Fabrication and Applications of Electronic Materials. Also scanning electron microscopy measurements were performed at Dokuz Eylul University in Izmir Biomedicine and Genome Centre (IBG). All authors would like to thank all.

References

- S.R. Anton, H.A. Sodano, *Smart Mater. Struct.* **16**, R1 (2007)
- D. Ai, H. Zhu, H. Luo, C. Wang, *Constr. Build. Mater.* **165**, 472 (2018)
- H. Kulkarni, K. Zohaib, A. Khusru, K. Shravan Aiyappa, *Mater Today* **5**, 21299 (2018)
- Z. Chen, Z. Wang, X. Li, Y. Lin, N. Luo, M. Long, N. Zhao, J. Bin Xu, *ACS Nano* **11**, 4507 (2017)
- T. Stevenson, D.G. Martin, P.I. Cowin, A. Blumfield, A.J. Bell, T.P. Comyn, P.M. Weaver, *J. Mater. Sci.* **26**, 9256 (2015)
- J. Briscoe, S. Dunn, *Nano Energy* **14**, 15 (2014)
- A. Shaji Karapuzha, N. Kunnamkuzhakkal James, S. van der Zwaag, W.A. Groen, *J. Mater. Sci.* **27**, 9683 (2016)
- S. Guan, H. Yang, G. Chen, R. Zhang, *J. Electron. Mater.* **47**, 2625 (2018)
- Y. Yoshino, *MRS Online Proceedings Library Archive*, vol. 518 (1998)
- M.-H. Zhao, Z.-L. Wang, S.X. Mao, *Nano Lett.* **4**, 587 (2004)
- S. Joshi, M.M. Nayak, K. Rajanna, *ACS Appl. Mater. Interfaces.* **6**, 7108 (2014)
- C. Dagdeviren, S. Hwang, Y. Su, S. Kim, H. Cheng, O. Gur, R. Haney, F.G. Omenetto, Y. Huang, J.A. Rogers, *Small* **9**, 3398 (2013)
- S.-H. Shin, M.H. Lee, J.-Y. Jung, J.H. Seol, J. Nah, *J. Mater. Chem. C* **1**, 8103 (2013)
- E. Lee, J. Park, M. Yim, S. Jeong, G. Yoon, *Appl. Phys. Lett.* **104**, 213908 (2014)
- C. Abels, V. Mastronardi, F. Guido, T. Dattoma, A. Qualtieri, W. Megill, M. De Vittorio, F. Rizzi, *Sensors* **17**, 1080 (2017)
- S. Petroni, F. Guido, B. Torre, A. Falqui, M.T. Todaro, R. Cingolani, M. De Vittorio, *Analyst* **137**, 5260 (2012)
- N. Jackson, L. Keeney, A. Mathewson, *Smart Mater. Struct.* **22**, 115033 (2013)
- F. Guido, A. Qualtieri, L. Algieri, E.D. Lemma, M. De Vittorio, M.T. Todaro, *Microelectron. Eng.* **159**, 174 (2016)
- K. Maity, D. Mandal, *ACS Appl. Mater. Interfaces.* **10**, 18257 (2018)
- X.-Q. Fang, J.-X. Liu, V. Gupta, *Nanoscale* **5**, 1716 (2013)
- A. Toprak, O. Tigli, *J. Mater. Sci.* **28**, 15877 (2017)
- D. Chen, T. Sharma, J.X.J. Zhang, *Sens. Actuators A* **216**, 196 (2014)
- T. Park, B. Kim, Y. Kim, E. Kim, *J. Mater. Chem. A* **2**, 5462 (2014)
- J. Zhao, Z. You, *Sensors* **14**, 12497 (2014)
- J.-H. Lee, K.Y. Lee, B. Kumar, N.T. Tien, N.-E. Lee, S.-W. Kim, *Energy Environ. Sci.* **6**, 169 (2013)
- C. Sun, J. Shi, D.J. Bayerl, X. Wang, *Energy Environ. Sci.* **4**, 4508 (2011)
- K. Sappati, S. Bhadra, *Sensors* **18**, 3605 (2018)
- A. Baji, Y.-W. Mai, Q. Li, Y. Liu, *Nanoscale* **3**, 3068 (2011)
- J. Yan, M. Liu, Y.G. Jeong, W. Kang, L. Li, Y. Zhao, N. Deng, B. Cheng, G. Yang, *Nano Energy* (2018)
- B. Dutta, E. Kar, N. Bose, S. Mukherjee, *RSC Adv.* **5**, 105422 (2015)
- J. Li, P. Khanchaitit, K. Han, Q. Wang, *Chem. Mater.* **22**, 5350 (2010)
- C. Xing, J. Guan, Y. Li, J. Li, *ACS Appl. Mater. Interfaces.* **6**, 4447 (2014)
- T. Hattori, M. Kanaoka, H. Ohigashi, *J. Appl. Phys.* **79**, 2016 (1996)
- K. Nakamura, D. Sawai, Y. Watanabe, D. Taguchi, Y. Takahashi, T. Furukawa, T. Kanamoto, *J. Polym. Sci. B* **41**, 1701 (2003)
- L. Kouchachvili, M. Ikura, *Int. J. Energy Res.* **32**, 328 (2008)
- Y.J. Yang, S. Aziz, S.M. Mehdi, M. Sajid, S. Jagadeesan, K.H. Choi, *J. Electron. Mater.* **46**, 4172 (2017)
- J. Fu, Y. Hou, M. Zheng, Q. Wei, M. Zhu, H. Yan, *ACS Appl. Mater. Interfaces.* **7**, 24480 (2015)
- R. Gregorio, M. Cestari, F.E. Bernardino, *J. Mater. Sci.* **31**, 2925 (1996)
- A.K. Batra, A. Alomari, M. McDaniel, K. Mckay, M. Creer, *Adv. Sci. Eng. Med.* **7**, 776 (2015)
- Y. Daben, *Ferroelectrics* **101**, 291 (1990)
- H. Banno, K. Ogura, *Ferroelectrics* **95**, 171 (1989)
- H.L.W. Chan, M.C. Cheung, C.L. Choy, *Ferroelectrics* **224**, 113 (1999)
- B. Wei, Y. Daben, *Ferroelectrics* **157**, 427 (1994)
- J.B. Ngoma, J.Y. Cavaille, J. Paletto, J. Perez, F. Macchi, *Ferroelectrics* **109**, 205 (1990)

45. Z. Dang, L. Wang, Y.I. Yin, Q. Zhang, Q. Lei, *Adv. Mater.* **19**, 852 (2007)
46. L. Wang, Z.-M. Dang, *Appl. Phys. Lett.* **87**, 42903 (2005)
47. A.K. Geim, K.S. Novoselov, in *Nanoscience and Technology: A Collection of Reviews from Nature Journals* (World Scientific, 2010), pp. 11–19
48. S. Park, R.S. Ruoff, *Nat. Nanotechnol.* **4**, 217 (2009)
49. Y. Zhu, S. Murali, W. Cai, X. Li, J.W. Suk, J.R. Potts, R.S. Ruoff, *Adv. Mater.* **22**, 3906 (2010)
50. T. Kuilla, S. Bhadra, D. Yao, N.H. Kim, S. Bose, J.H. Lee, *Prog. Polym. Sci.* **35**, 1350 (2010)
51. S.M. Azeem, M.T. Saleem, M. Faizan, S. Ahmed, I. Masood, in *Key Engineering Materials* (Trans Tech Publ, 2018), pp. 144–150
52. A.A. Isari, A. Payan, M. Fattahi, S. Jorfi, B. Kakavandi, *Appl. Surf. Sci.* **462**, 549 (2018)
53. H. Kim, Y. Miura, C.W. MacOsco, *Chem. Mater.* **22**, 3441 (2010)
54. L. Teresa, M. Gámez, *J. Polym. Sci.* **45**, 2007 (2007)
55. C.M. Wu, M.H. Chou, *Eur. Polym. J.* **82**, 35 (2016)
56. R.K. Layek, S. Samanta, D.P. Chatterjee, A.K. Nandi, *Polymer* **51**, 5846 (2010)
57. S. Ansari, E.P. Giannelis, *J. Polym. Sci. B* **47**, 888 (2009)
58. L. Wu, J. Alamusi, T. Xue, N. Itoi, Y. Hu, C. Li, J. Yan, H. Qiu, Ning, W. Yuan, *J. Intell. Mater. Syst. Struct.* **25**, 1813 (2014)
59. J.S. Lee, K.-Y. Shin, C. Kim, J. Jang, *Chem. Commun.* **49**, 11047 (2013)
60. J. Xue, L. Wu, N. Hu, J. Qiu, C. Chang, S. Atobe, H. Fukunaga, T. Watanabe, Y. Liu, H. Ning, *Nanoscale* **4**, 7250 (2012)
61. M.A. Rahman, B.-C. Lee, D.-T. Phan, G.-S. Chung, *Smart Mater. Struct.* **22**, 85017 (2013)
62. M.M. Abolhasani, K. Shirvanimoghaddam, M. Naebe, *Compos. Sci. Technol.* **138**, 49 (2017)
63. Y. Chen, Y. Niu, T. Tian, J. Zhang, Y. Wang, Y. Li, L.-C. Qin, *Chem. Phys. Lett.* **677**, 143 (2017)
64. D.S. Gyan, A. Dwivedi, *J. Appl. Phys.* **125**, 24103 (2019)
65. P. Martins, A.C. Lopes, S. Lanceros-Mendez, *Prog. Polym. Sci.* **39**, 683 (2014)
66. S. Garain, S. Jana, T.K. Sinha, D. Mandal, *ACS Appl. Mater. Interfaces* **8**, 4532 (2016)
67. S.-D. Wang, Q. Ma, K. Wang, H.-W. Chen, *ACS Omega* **3**, 406 (2018)
68. C. Wu, X. Huang, L. Xie, X. Wu, J. Yu, P. Jiang, *J. Mater. Chem.* **21**, 17729 (2011)
69. J.-K. Yuan, Z.-M. Dang, S.-H. Yao, J.-W. Zha, T. Zhou, S.-T. Li, J. Bai, *J. Mater. Chem.* **20**, 2441 (2010)
70. J. Shang, Y. Zhang, L. Yu, B. Shen, F. Lv, P.K. Chu, *Mater. Chem. Phys.* **134**, 867 (2012)
71. J. Shang, Y. Zhang, L. Yu, X. Luan, B. Shen, Z. Zhang, F. Lv, P.K. Chu, *J. Mater. Chem. A* **1**, 884 (2013)
72. W. Tong, Y. Zhang, L. Yu, X. Luan, Q. An, Q. Zhang, F. Lv, P.K. Chu, B. Shen, Z. Zhang, *J. Phys. Chem. C* **118**, 10567 (2014)
73. T. Liu, P.H. Zhou, J.L. Xie, L.J. Deng, *J. Appl. Phys.* **110**, 33918 (2011)
74. X.-J. Zhang, G.-S. Wang, W.-Q. Cao, Y.-Z. Wei, M.-S. Cao, L. Guo, *RSC Adv.* **4**, 19594 (2014)
75. M.El Achaby, F.Z. Arrakhiz, S. Vaudreuil, E.M. Essassi, A. Qaiss, *Appl. Surf. Sci.* **258**, 7668 (2012)

Publisher's Note Springer Nature remains neutral with regard to jurisdictional claims in published maps and institutional affiliations.